

The present reaction is of general importance for conservative self-organization processes with formation of complex structures from more simple ones. It can be concluded that in polyoxometalate systems a stepwise growth process can take place, whereby an initial cluster acts as a compartment for the aggregation of additional building units to form clusters that are not stable on their own (see also ref. 10). The aggregation of units within the cavity of the $\{\text{Mo}_{176}\}$ cluster can be regarded as a model both for crystal growth (especially for the initial nucleation process, which is still not understood) and also for metal-centre assembly processes in biological systems. In particular such growth processes might be allied to biomineralization in compartments or to metal-centre uptake in metal-storage proteins, such as the formation of the polyoxometalate nucleus of the molybdenum storage protein of the N_2 -fixing microorganisms *Azotobacter vinelandii*¹¹. □

Methods

Synthesis of 1a. An aqueous solution of 3 g of Na_2MoO_4 (12.5 mmol) in 45 ml H_2O is acidified with 2.5 ml of 32% HCl under continuous stirring. After adding 1.2 ml of ascorbic acid solution (0.5 M, 0.6 mmol), within a few minutes the reaction mixture turns yellow, then green, and finally dark blue. The reaction flask was covered with a stopper and allowed to stand for 4–5 weeks for crystallization (yield 0.38 g; correct analysis).

Selected physical data. Infrared (KBr pellet): ν (cm^{-1}) = 1,610 $\{\text{m}, \delta(\text{H}_2\text{O})\}$, 976(w), 914(m) $\{\nu$ (MoO) $\}$, 745(s), 629(m), 557(s); resonance-Raman (KBr pellet): ν (cm^{-1}) = 946 (m), 791(s), 540(m), 464(s), 327(s), 215(s); near-infrared/visible (in 40% MeOH/ H_2O for the estimation of the (formal) number of Mo^{V} centres): λ (nm) (ϵ_{M}) = 753 ($3.5 \times 10^5 \text{ l mol}^{-1} \text{ cm}^{-1}$), 1,016 ($2.5 \times 10^5 \text{ l mol}^{-1} \text{ cm}^{-1}$).

X-ray structure analysis. Space group $C22_1$, $a = 53.835(4)$, $b = 31.505(2)$, $c = 66.818(5)$ Å, $V = 113329(15)$ Å³, $Z = 4$, $\rho = 2.279 \text{ g cm}^{-3}$, $\mu = 2.38 \text{ mm}^{-1}$, $F(000) = 74,512$, crystal size = $0.28 \times 0.28 \times 0.10 \text{ mm}$. Crystals were removed from the mother liquor and immediately cooled to 183(2) K on a Bruker axis SMART diffractometer (Mo-K α , graphite monochromator). A total of 185,373 reflections ($1.83^\circ < \theta < 22.49^\circ$) were collected, of which 71,853 unique reflections ($R_{\text{int}} = 0.085$) were used. The structure was solved using the program SHELXS-97 and refined (3,333 parameters) using the program SHELXL-97 to $R = 0.0751$ for 35,731 reflections with $I > 2\sigma(I)$ (both programs from G. M. Sheldrick, Univ. Göttingen, 1997). The Na^+ ions, as well as several crystal water molecules, could not be localized due to their disorder.

Received 31 July; accepted 15 September 1998.

- Müller, A. & Pope, M. T. in *From Simplicity to Complexity Part II: Information—Interaction—Emergence* (eds Mainzer, K., Müller, A. & Saltzer, W. G.) 57–68 (Vieweg, Braunschweig, 1998).
- Pope, M. T. & Müller, A. Polyoxometalate chemistry: an old field with new dimensions in several disciplines. *Angew. Chem. Int. Edn Engl.* **30**, 34–48 (1991).
- Rhule, J. T., Hill, C. L., Judd, D. A. & Schinazi, R. F. Polyoxometalates in medicine. *Chem. Rev.* **98**, 327–357 (1998).
- Katsoulis, D. E. A survey of applications of polyoxometalates. *Chem. Rev.* **98**, 359–387 (1998).
- Müller, A. et al. $[\text{Mo}_{154}(\text{NO})_{10}(\text{OH})_{28}(\text{H}_2\text{O})_{70}]^{(25-)}:$ a water-soluble big wheel with more than 700 atoms and a relative molecular mass of about 24000. *Angew. Chem. Int. Edn Engl.* **34**, 2122–2124 (1995).
- Müller, A., Peters, E., Pope, M. T. & Gatteschi, D. Polyoxometalates: very large clusters—nanoscale magnets. *Chem. Rev.* **98**, 239–271 (1998).
- Müller, A. et al. Formation of a ring-shaped reduced ‘metal oxide’ with the simple composition $[(\text{MoO}_3)_{176}(\text{H}_2\text{O})_{80}\text{H}_{12}]$. *Angew. Chem. Int. Edn Engl.* **37**, 1220–1223 (1998).
- Müller, A., Koop, M., Bögge, H., Schmidtman, M. & Beugholt, C. Exchanged ligands on the surface of a giant cluster: $[(\text{MoO}_3)_{176}(\text{H}_2\text{O})_{80}(\text{CH}_3\text{OH})_{17}\text{H}_n]^{(92-)}$. *J. Chem. Soc., Chem. Commun.* 1501–1502 (1998).
- Williams, N. H. & Yandell, J. K. Outer-sphere electron-transfer reactions of ascorbate anions. *Aust. J. Chem.* **35**, 1133–1144 (1982).
- Müller, A. et al. Unusual stepwise assembly and molecular growth: $[\text{H}_{14}\text{Mo}_{37}\text{O}_{112}]^{14-}$ and $[\text{H}_3\text{Mo}_{57}\text{V}_6(\text{NO})_6\text{O}_{189}(\text{H}_2\text{O})_{12}(\text{MoO}_6)]^{21-}$. *Chem. Eur. J.* **4**, 1000–1006 (1998).
- Müller, A. et al. Comparative *in-vivo* and *in-vitro* ⁹⁹Mo-time-differential-perturbed-angular-correlation studies on the nitrogenase MoFe protein and on other Mo species of different N_2 -fixing bacteria. *Eur. J. Biochem.* **246**, 311–319 (1997).
- Robin, M. B. & Day, P. Mixed valence chemistry - a survey and classification. *Inorg. Chem. Radiochem.* **10**, 247–422 (1967).

Acknowledgements. We thank E. Krickemeyer, B. Hauptfleisch, C. Beugholt, E. Diemann and F. Peters for their collaboration. This work was supported by the Deutsche Forschungsgemeinschaft and the Fonds der Chemischen Industrie.

Correspondence and requests for materials should be addressed to A.M. (e-mail: a.mueller@uni-bielefeld.de). Further details of crystal structure determination may be obtained from the Fachinformationszentrum Karlsruhe, D-76344 Eggenstein-Leopoldshafen, Germany, on quoting the depository no. CSD 410267, names of authors and journal citation.

Energy landscapes of receptor–ligand bonds explored with dynamic force spectroscopy

R. Merkel*†, P. Nassoy*‡, A. Leung*, K. Ritchie* & E. Evans*§

* Departments of Physics and Pathology, University of British Columbia, Vancouver, British Columbia, Canada V6T 1Z1

† Physikdepartment der Technischen Universität München, 85748 Garching, Germany

‡ Physico-Chemie de l’Institut Curie, 75231 Paris, France

§ Biomedical Engineering, Boston University, Boston, Massachusetts 02215, USA

Atomic force microscopy (AFM)^{1,2} has been used to measure the strength of bonds between biological receptor molecules and their ligands^{3–6}. But for weak noncovalent bonds, a dynamic spectrum of bond strengths is predicted as the loading rate is altered, with the measured strength being governed by the prominent barriers traversed in the energy landscape along the force-driven bond-dissociation pathway⁷. In other words, the pioneering early AFM measurements represent only a single point in a continuous spectrum of bond strengths, because theory predicts that these will depend on the rate at which the load is applied. Here we report the strength spectra for the bonds between streptavidin (or avidin) and biotin⁸—the prototype of receptor–ligand interactions used in earlier AFM studies^{3–5}, and which have been modelled by molecular dynamics^{9,10}. We have probed bond formation over six orders of magnitude in loading rate, and find that the bond survival time diminished from about 1 min to 0.001 s with increasing loading rate over this range. The bond strength, meanwhile, increased from about 5 pN to 170 pN. Thus, although they are among the strongest noncovalent linkages in biology (affinity of 10^{13} to 10^{15} M^{-1})^{8,11}, these bonds in fact appear strong or weak depending on how fast they are loaded. We are also able to relate the activation barriers derived from our strength spectra to the shape of the energy landscape derived from simulations of the biotin–avidin complex.

To measure strengths, we used two modes of a biomembrane force probe (BFP)¹² as described in Fig. 1 legend: a vertical mode with high resolution in position and force (2–5 nm and 0.2–0.5 pN) for testing weak bonds under slow loading (Fig. 2a); and a horizontal mode with modest resolution (8–10 nm and 1–10 pN) for testing strong bonds under fast loading (Fig. 2b). The BFP tip and test surface were prepared with a paucity of reactive sites to limit the frequency of bond formation to 1 per 7–10 touches in the tests (see Methods). As such, the likelihood of forming and breaking single bonds was expected to be greater than 0.9. To obtain sufficient numbers (50–100) of rupture forces at each loading rate, several hundred cycles of approach–touch–separation were performed by computer-controlled piezo displacement of either the transducer or the test surface. The nominal loading rate k_{FV} was preselected by setting the BFP force constant k_{f} in the range 0.1–3 pN nm⁻¹ and piezo retraction speed v_{t} in the range 1–20,000 nm s⁻¹. Force histograms were compiled at 11 and 8 loading rates between 0.05 to 60,000 pN s⁻¹ for biotin–avidin and biotin–streptavidin, respectively. A montage of histograms is shown in Fig. 3a for biotin–streptavidin. Complete spectra of the most frequent rupture forces f^* versus $\log r_{\text{f}}$ (where r_{f} = loading rate) are plotted in Fig. 3b.

To understand why strength depends on loading rate, it is important to recognize that the lifetime of a bond sustained by weak noncovalent interactions diminishes rapidly when subjected to force because of thermal activation. Conceptually, the energy landscape is tilted by force (Fig. 4a), which lowers energy barriers,

decreases the likelihood of bond survival, and speeds up dissociation. So, we might expect the form of a strength spectrum obtained under rising force in probe tests to be complicated and difficult to interpret. However, when linear regimes appear over many orders of magnitude of loading rate as in Fig. 3b, interpretation of the spectrum is simple: each regime produces an image of a sharp energy barrier at a fixed location along the unbinding pathway⁷. The energy contour in configuration space local to a sharp barrier (called the transition state) is highly curved and therefore does not change shape as the barrier height falls under rising force f (Fig. 4a). The thermally averaged displacement in configuration space needed to reach the top of the barrier does not shift with force and the displacement maps to a constant position x_β along the direction of force. First postulated intuitively by Bell¹³, lowering the barrier by the mechanical potential fx_β leads to exponential amplification of the dissociation kinetics, that is, off rate $\nu \approx \nu_0 \exp(fx_\beta/k_B T)$. Hence, the relevant force scale $f_\beta = k_B T/x_\beta$ for thermally activated rupture is thermal energy ($k_B T \approx 4.1 \times 10^{-21}$ J or ≈ 4.1 pN nm at room temperature) divided by the projected bond displacement, not the maximum gradient in an energy landscape. The force statistics in probe tests are predicted by a first-order kinetic process where dissociation rate increases rapidly with the rising force⁷. For a single barrier, the peak f^* in the force distribution shifts to higher force in proportion to \log_e (loading rate) with a slope f_β . Much less trivial,

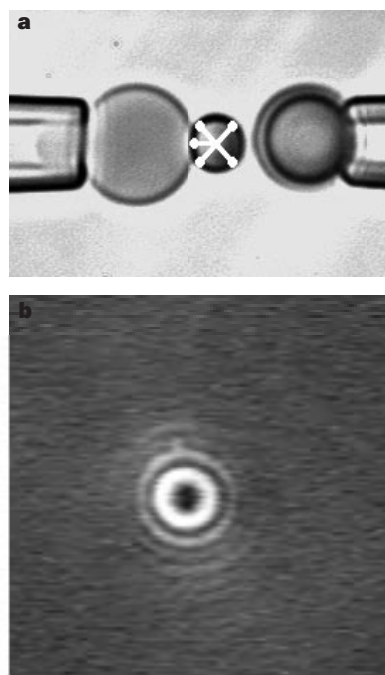


Figure 1 The spring in the biomembrane force probe BFP is a pressurized membrane capsule¹². Membrane tension sets the force constant k_f (force/capsule extension) and is controlled by micropipette suction P and radius R_p , $k_f \sim PR_p$. Using a red blood cell as the transducer, the BFP stiffness was tuned between 0.1 and 3 pN nm⁻¹ to measure forces from 0.5 to 1,000 pN. As the BFP tip, a glass microbead of 1–2 μm diameter was chemically glued to the membrane (see Methods). **a**, Operated on the stage of an inverted microscope, the BFP (on the left) in the horizontal mode was kept stationary and the microbead test surface (on the right) was translated to/from contact with the BFP tip by precision piezo control. With fast video ($\sim 1,000$ frames per s) processing, a simulated cursor was required to track the image of the bead as shown, which yielded a resolution of 8–10 nm for transducer deflection. **b**, Reflection interference contrast image of the BFP tip translated along the optical axis by piezo control to/from a coverglass test surface in the vertical mode. Standard video (30 frames per s) processing of the circular interference pattern was used to track elevation of the tip at a resolution of 2–5 nm. Transducer deflection was obtained from the difference between piezo translation and bead displacement.

complex macromolecular bonds involve many interactions that create a mountainous terrain of barriers in the energy landscape. Assuming a cascade of sharp barriers, the strength spectrum is predicted to follow a piece-wise continuous sequence of linear regimes with ascending slopes⁷. The abrupt increase in slope from one regime to the next signifies that an outer barrier has been suppressed by force and that an inner barrier becomes the dominant kinetic impedance, as shown in Fig. 4a. The regime governed by a particular barrier spans a range of \log_e (loading rate) determined by its height relative to adjacent barriers (see Methods). The off rate rises as a staircase of exponentials in force that amplify off rate less and less from one to the next.

Applying these concepts to the spectra plotted in Fig. 3b, we derive locations of prominent energy barriers that govern strength of biotin–streptavidin and biotin–avidin bonds. How does this one-dimensional map along the direction of probe force compare with detailed molecular dynamics (MD) simulations of biotin–(strept)avidin interactions? In separate simulations, biotin was extracted from a binding pocket of streptavidin⁹ and avidin¹⁰ by pulling on the outer end with a pseudo-mechanical spring. Chemically and structurally, the binding pockets in avidin and streptavidin are very similar except biotin forms an additional nonpolar interaction and three additional hydrogen bonds in avidin^{14,15}. Also, the longer ‘3–4’ loop in avidin seems to close more tightly behind biotin in the bound state^{14–16}. Revealing the inherent molecular complexity, the simulations yield a dynamic superposition of many polar (hydrogen bonds and water bridges) and nonpolar (to aromatic residues) interactions along the unbinding trajectories, which are emphasized quite differently in each report^{9,10}. Even so, common qualitative features are described that provide important clues to the thermally averaged free energy landscape relevant on laboratory timescales. First, within an initial displacement of less than 0.2 nm, unbinding began with detachment of the ‘head’ (ureido ring) of

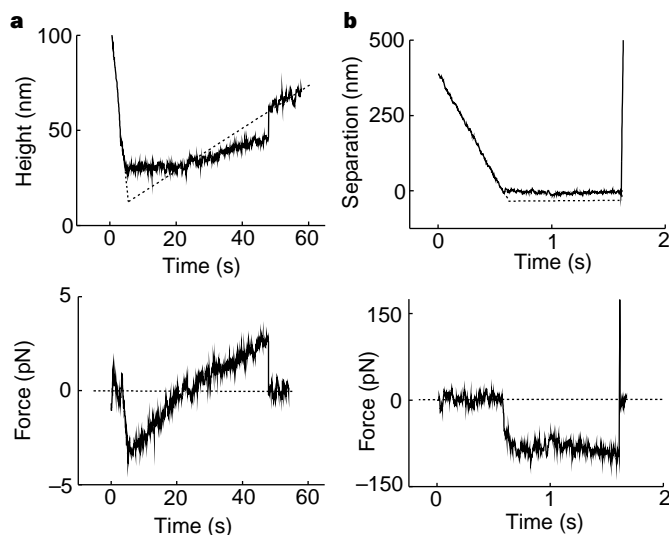


Figure 2 BFP tip–substrate distance and force versus time for cycles of approach–touch–separation with formation and rupture of a bond. **a**, Loaded at extremely slow rate, a bond held the tip to the surface for ~ 24 s and broke at ~ 3 pN as the piezo retracted the transducer (dashed trajectory). The fluctuations in tip position were due to thermal excitations of the BFP (mean square displacement $\sim k_B T/k_f$). Stretch of the PEG polymers that linked the bond to the glass surfaces is shown by the slight upward movement (~ 15 nm) under force before detachment. Because of polymer compliance, the true loading rate felt by a bond at nominal rates ($k_f v_t$) below 10 pN s⁻¹ had to be obtained from the force versus time. **b**, Loaded at extremely fast rate, a bond held the tip to the surface for ~ 0.003 s (spike in force) and broke at ~ 170 pN as the piezo retracted the test surface (dashed trajectory). The force fluctuations were due to position uncertainties \times BFP stiffness.

biotin from a nest of hydrogen bonds, water bridges and nonpolar interactions deep in the binding pocket. Next, forces reached maximal values followed by sudden displacements of biotin at a distance of ~ 0.5 nm in the biotin–streptavidin simulation (attributed to rupture in a transient network of water bridges and hydrogen bonds) and at ~ 0.4 nm in the biotin–avidin simulation (attributed both to polar and to nonpolar interactions). Finally, as biotin left the pocket, a prominent jump occurred with lower forces at ~ 1 nm in both simulations (attributed to hydrogen bonds) and biotin was observed still to cling to peripheral polar groups at ~ 1.4 nm in avidin simulations. To show this behaviour clearly, we have plotted a record of the instantaneous interaction energies between biotin and avidin calculated over a half-nanosecond time course of extraction in the simulations of Israilev *et al.*¹⁰ (Fig. 4b).

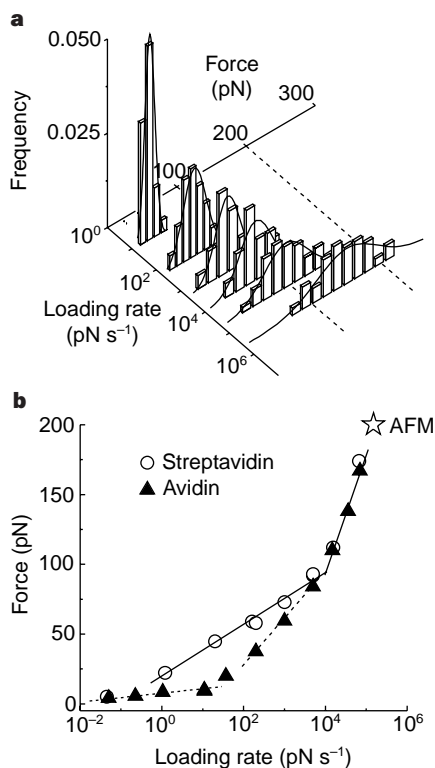


Figure 3 Biotin–streptavidin bond strengths. **a**, Force histograms from tests of single biotin–streptavidin bonds demonstrate shift in peak location and increase in width with increase in loading rate. Gaussian fits used to determine the most frequent rupture force or bond strength are shown. Governed ideally by the thermal force f_β , standard deviations σ_f of the distributions also reflected uncertainties in position Δx and video sampling time Δt_v , that is, $\sigma_f \sim [f_\beta^2 + (k_f \Delta x)^2 + (r_f \Delta t_v)^2]^{1/2}$. As σ_f increased from ± 1 pN at the slowest rate to ± 60 pN at the fastest rate, the standard error in mean force (the statistical measure for error in strength) ranged from ± 0.3 pN to ± 5 pN. **b**, Dynamic strength spectra for biotin–streptavidin (circles) and biotin–avidin (triangles) bonds. Defined as thermal energy $k_B T \div$ distance x_β , the slopes (f_β) of the solid lines in the biotin–streptavidin spectrum map activation barriers at $x_\beta \approx 0.5$ nm and 0.12 nm along the direction of force based on values of 8 pN and 34 pN. Merging with biotin–streptavidin above 85 pN, the high-strength regime for biotin–avidin also maps an inner barrier at $x_\beta \approx 0.12$ nm but the slope $f_\beta \approx 13$ – 14 pN of the intermediate strength regime (dashed line) between 38 pN and 85 pN indicates that the next barrier maps to $x_\beta \approx 0.3$ nm. Slight curvature and reduction in slope between 38 pN and 11 pN suggests that the barrier extends to ~ 0.5 nm. Below 11 pN, the biotin–avidin spectrum exhibits a low-strength regime (dashed line) with a slope of $f_\beta \approx 1.4$ pN that maps to $x_\beta \approx 3$ nm. Consistent with the high-strength regime is the biotin–streptavidin strength (\star_{AFM}) measured recently by atomic-force microscopy (AFM) using a carbon nanotube as the tip²⁴ and the biotin–avidin strength (not shown) measured previously⁴ by AFM.

Transition states are readily identified by regions with a paucity of states where biotin passes quickly. Marked in Fig. 4b, the activation barriers derived from the high and intermediate strength regimes in Fig. 3b correlate with regions of rarified statistics and the qualitative appearance of the energy landscape. The interpretation is that the transition states implied by these features persist on long timescales and that the molecular reaction coordinate perhaps deviates by ~ 40 – 45° from the direction of force local to the second transition state. But surprisingly, the outer barrier indicated by the low-strength regime in Fig. 3b is 2–3-fold more distant than the last transition state seen in the MD simulation.

Guided by the MD simulation, we expect the outer barrier to emanate from molecular interactions with the flexible ‘3–4’ loop, which closes behind biotin in crystallographic images^{14–16} of the

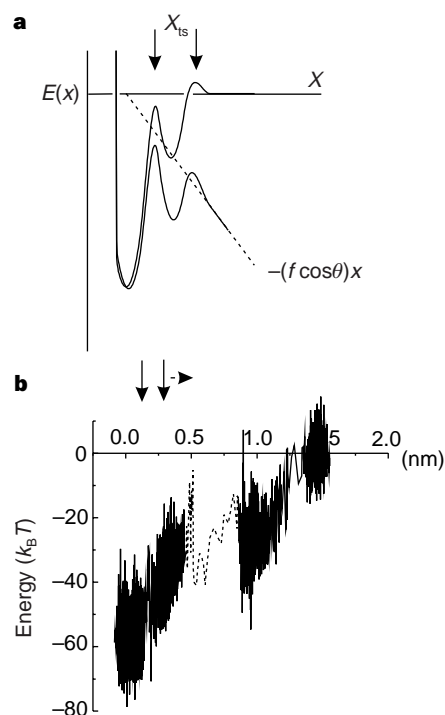


Figure 4 Conceptual and real (MD) energy landscapes traversed along a molecular reaction coordinate under force. **a**, Oriented at an angle θ to the molecular coordinate x , external force f adds a mechanical potential, $-(f \cos \theta)x$, that tilts the landscape and lowers barriers. The inner barrier emerges to dominate kinetics when the outer barrier falls to a level $\geq k_B T$ below it under force. For sharp barriers, the local energy contours, called transition states, are highly curved and change little in shape or location under force. Even though the unbinding pathway may be tortuous and the orientation fluctuates wildly, the energy weighted locations of sharp barriers can project as constant distances $x_\beta = (x_\beta \cos \theta)$ along the direction of force. **b**, Instantaneous interaction energy between biotin and avidin computed along a half-nanosecond extraction from the binding pocket in the simulations of Israilev *et al.*¹⁰ (kindly provided to us by K. Schulten and co-workers, University of Illinois). Bordered by regions of rapid intense fluctuations, locations of rarified statistics reveal transition states expected in a thermally averaged free energy landscape⁷. Arrows mark barrier locations derived from the strength spectrum for biotin–avidin in Fig. 3b.

bound state and was set in an open conformation in MD simulations. Consistent with this expectation, mutations that delete the '3-4' loop in streptavidin result in major reductions in magnitude of binding enthalpy^{16,17}. Interestingly, in the absence of biotin, the '3-4' loop disappears in crystallographic images indicating that the loop becomes disordered and flexible. Moreover, although not currently implicated in biotin-avidin binding, other longer loops also border the channel that leads to the binding pocket. Thus, our speculation is that the outer barrier at ~3 nm represents interactions on laboratory timescales of the spacer-linked biotin with soft, flexible elements well beyond the binding pocket. Even though biotin-(strept)avidin bonds can break under very small forces, the location of the outer barrier at ~3 nm leads to a significant difference in energy between the outer and nearby inner barriers as indicated by the difference in log/loading rate intercepts of the low and intermediate strength regimes.

The profound effect of thermal activation on strength of non-covalent linkages in biology has been recognized by researchers studying cell adhesion dynamics in shear flow^{18,19} and recently also in the unfolding of tandem immunoglobulin-like domains in long proteins^{20,21}. What is not well known, however, is that thermal activation in a complex biomolecular assembly is likely to be governed by a rugged energy landscape with more than one kinetic barrier. We have shown here that to explore such a landscape with force probes, experiments have to be performed over an enormous range of loading rates. □

Methods

Chemical preparation of BFP tips and test surfaces. First, amino silane (AEAPTMS, United Chemical Technologies, PA) groups were covalently bound to glass microbeads and coverslips. Next, amine-reactive polyethylene oxide polyethylene glycol (PEG) polymers with and without biotin end groups (mixture of NHS-PEG3400-VS and NHS-PEG3400-biotin, Shearwater Polymers, AL) were covalently linked to the silanized surfaces. Finally, the biotinylated beads and coverglasses were exposed to excess (strept)avidin and then washed. Even though almost completely saturated with (strept)avidin, the surfaces still had a number of free biotin groups. Thus, bonds formed very infrequently when identically prepared tip and test surfaces were touched together. (No bonding was detected when the PEG polymers on the test surface were terminated with methyl groups or when free biotin was blown at the tip and test surface by an auxiliary micropipette before touch.) A red cell covalently linked with PEG-biotin polymers was pushed together with an avidinated microbead to construct the probe as shown in Fig. 1a.

Analysis of strength spectra. Slopes of linear regimes in strength versus log_e(loading rate) map energy barriers to fixed distances x_{β} along the direction of force⁷. Each slope is the force scale $f_{\beta} = k_B T/x_{\beta}$ for e-fold amplification of dissociation rate impeded by a particular barrier. Barriers emerge in succession from outer to inner positions to dominate kinetics. Reflecting the Arrhenius dependence in the off rate, $v_0 = (1/t_D)\exp(-E_b/k_B T)$, differences in logarithmic intercept $\log_e(r_f)_{r=0}$ and slope f_{β} of regimes in Fig. 3b expose differences in barrier heights, $\Delta E_b \approx k_B T\{\Delta \log_e[f_{\beta}/t_D] - \Delta \log_e(r_f)_{r=0}\}$, within an unknown variation in a diffusive relaxation time t_D . Worked out by Kramers^{22,23}, the frequency $1/t_D$ in liquids is governed by viscous friction γ_f and a product of length scales l_{aTs} ($l_a \equiv$ confinement length in the bound state and $l_s \equiv$ impedance width of the transition state), that is, $1/t_D \approx k_B T/(\gamma_f l_a l_s)$ and $k_B T/\gamma_f$ defines a diffusivity. From MD simulations⁹, values of $\gamma_f \sim 2 \times 10^{-8}$ pN s nm⁻¹ and $x_{\beta} x_{Ts} \sim 0.01-0.1$ nm² imply that $1/t_D$ is $\sim 10^9-10^{10}$ s⁻¹ and that $\log_e(f_{\beta}/t_D)$ is $\sim 21-25$ for a rate scale in pN s⁻¹.

6. Hinterdorfer, P., Baumgartner, W., Gruber, H. J., Schilcher, K. & Schindler, H. Detection and localization of individual antibody-antigen recognition events by atomic force microscopy. *Proc. Natl Acad. Sci. USA* **93**, 3477-3481 (1996).
7. Evans, E. & Ritchie, K. Dynamic strength of molecular adhesion bonds. *Biophys. J.* **72**, 1541-1555 (1997).
8. Green, N. M. Avidin. *Adv. Protein Chem.* **29**, 85-133 (1975).
9. Grubmuller, H., Heymann, B. & Tavan, P. Ligand binding: molecular mechanics calculation of the streptavidin-biotin rupture force. *Science* **271**, 997-999 (1996).
10. Izrailev, S., Stepaniants, S., Balsera, M., Oono, Y. & Schulten, K. Molecular dynamics study of unbinding of the avidin-biotin complex. *Biophys. J.* **72**, 1568-1581 (1997).
11. Chilkoti, A. & Stayton, P. S. Molecular origins of the slow streptavidin-biotin dissociation kinetics. *J. Am. Chem. Soc.* **117**, 10622-10628 (1995).
12. Evans, E., Ritchie, K. & Merkel, R. Sensitive force technique to probe molecular adhesion and structural linkages at biological interfaces. *Biophys. J.* **68**, 2580-2587 (1995).
13. Bell, G. I. Models for the specific adhesion of cells to cells. *Science* **200**, 618-627 (1978).
14. Weber, P. C., Ohlendorf, D. H., Wendoloski, J. J. & Salemme, F. R. Structural origins of high-affinity biotin binding to streptavidin. *Science* **243**, 85-88 (1989).
15. Livnah, O., Bayer, E. A., Wilchek, M. & Sussman, J. L. Three-dimensional structures of avidin and the avidin-biotin complex. *Proc. Natl Acad. Sci. USA* **90**, 5076-5080 (1993).
16. Freitag, S., Le Trong, I., Klumb, L., Stayton, P. S. & Stenkamp, R. E. Structural studies of the streptavidin binding loop. *Protein Sci.* **6**, 1157-1166 (1997).
17. Chu, V., Freitag, S., Le Trong, I., Stenkamp, R. E. & Stayton, P. S. Thermodynamic and structural consequences of flexible loop deletion by circular permutation in the streptavidin-biotin system. *Protein Sci.* **7**, 848-859 (1998).
18. Alon, R., Hammer, D. A. & Springer, T. A. Lifetime of the P-selectin-carbohydrate bond and its response to tensile force in hydrodynamic flow. *Nature* **374**, 539-542 (1995).
19. Brunk, D. K., Goetz, D. J. & Hammer, D. A. Sialyl Lewis^x/E-selectin-mediated rolling in a cell-free system. *Biophys. J.* **71**, 2902-2907 (1996).
20. Rief, M., Gautel, M., Osterhelt, F., Fernandez, J. M. & Gaub, H. E. Reversible unfolding of individual titin immunoglobulin domains by AFM. *Science* **276**, 1109-1112 (1997).
21. Oberhauser, A. F., Marszalek, P. E., Erickson, H. P. & Fernandez, J. M. The molecular elasticity of the extracellular matrix protein tenascin. *Nature* **393**, 181-185 (1998).
22. Kramers, H. A. Brownian motion in a field of force and the diffusion model of chemical reactions. *Physica (Utrecht)* **7**, 284-304 (1940).
23. Hanggi, P., Talkner, P. & Borkovec, M. Reaction-rate theory: fifty years after Kramers. *Rev. Mod. Phys.* **62**, 251-342 (1990).
24. Wong, S. S., Joselivich, E., Woolley, A. T., Cheung, C. L. & Lieber, C. M. Covalently functionalized nanotubes as nanometre-sized probes in chemistry and biology. *Nature* **394**, 52-55 (1998).

Acknowledgements. We thank A. Chilkoti, C. Cantor and the group of K. Schulten for helpful discussions. The work was supported by USPHS National Institutes of Health, Medical Research Council of Canada, and the Canadian Institute for Advanced Research Program in Science of Soft Surfaces and Interfaces.

Correspondence and request for materials should be addressed to E.E. (e-mail: evans@physics.ubc.ca).

The fate of subducted basaltic crust in the Earth's lower mantle

Kei Hirose*, Yingwei Fei, Yanzhang Ma & Ho-Kwang Mao

Geophysical Laboratory and Center for High Pressure Research, Carnegie Institution of Washington, 5251 Broad Branch Road NW, Washington DC 20015, USA

* Present address: Department of Earth and Planetary Sciences, Tokyo Institute of Technology, Ookayama, Tokyo 152-8551, Japan

The subduction of oceanic lithosphere into the Earth's deep interior is thought to drive convection and create chemical heterogeneity in the mantle. The oceanic lithosphere as a whole, however, might not subduct uniformly: the fate of basaltic crust may differ from that of the underlying peridotite layer because of differences in chemistry, density and melting temperature. It has been suggested that subducted basaltic crust may in fact become buoyant at the mantle's 660-km discontinuity, remaining buoyant to depths of at least 800 km, and therefore might be gravitationally trapped at this boundary to form a garnetite layer^{1,2}. Here we report the phase relations and melting temperatures of natural mid-ocean ridge basalt at pressures up to 64 GPa (corresponding to ~1,500 km depth). We find that the former basaltic crust is no longer buoyant when it transforms to a perovskite lithology at about 720 km depth, and that this transition boundary has a positive pressure-temperature slope, in contrast to the negative slope of the transition boundary in peridotite. We therefore predict that basaltic crust with perovskite lithology would gravitationally sink into the deep mantle. Our melting data suggest that, at the base of the lower mantle, the former basaltic

Received 5 May; accepted 5 October 1998.

1. Binnig, G., Quate, C. F. & Gerber, C. H. Atomic force microscopy. *Phys. Rev. Lett.* **56**, 930-933 (1986).
2. Drake, B. et al. Imaging crystals, polymers, and processes in water with the atomic force microscope. *Science* **243**, 1586-1589 (1989).
3. Lee, G. U., Kidwell, D. A. & Colton, R. J. Sensing discrete streptavidin-biotin interactions with atomic force microscopy. *Langmuir* **10**, 354-357 (1994).
4. Florin, E.-L., Moy, V. T. & Gaub, H. E. Adhesive forces between individual ligand receptor pairs. *Science* **264**, 415-417 (1994).
5. Moy, V. T., Florin, E.-L. & Gaub, H. E. Intermolecular forces and energies between ligands and receptors. *Science* **264**, 257-259 (1994).